

# Sulfa Guanidine Azo Derivatives as Environmentally - Friendly Corrosion Inhibitors for Nickel in HCl Solution: Theoretical and Experimental Study

Hala.M.Hassan<sup>1\*</sup>, A.M.Eldesoky<sup>2</sup> and Wael A. Zordok<sup>3</sup>

<sup>1</sup>Textile Technology Department, Industrial Education College, Beni-Suef University, Egypt and Chemistry Department, Faculty of Science, Jazan University, KSA.

<sup>2</sup>Engineering Chemistry Department, High Institute of Engineering & Technology (New Damietta), Egypt and Al-Qunfudah Center for Scientific Research (QCSR), Al-Qunfudah University College, Umm Al-Qura University, KSA.

<sup>3</sup>Department of Chemistry, Faculty of Science, Zagazig University, Zagazig, Egypt and Department of Chemistry University College of Qunfudha, Umm Al -Qura University, KSA.

**Abstract-**The protection influence of three sulfa guanidine azo derivatives against nickel corrosion was studied in 0.5 M HCl solutions at 25°C. Measurements were conducted under various experimental conditions using potentiodynamic polarization, electrochemical impedance spectroscopy (EIS) and electrochemical frequency modulation (EFM) techniques. These studies have shown that sulfa guanidine azo derivatives are very good “green”, mixed-type inhibitors. Electrochemical frequency modulation (EFM) and electrochemical impedance spectroscopy (EIS) method of analysis are also presented here for monitoring corrosion. Corrosion rates obtained from both EFM and EIS methods are comparable with those recorded using Tafel extrapolation method, confirming validation of corrosion rates measured by the latter. The inhibitive action of these sulfa guanidine azo derivatives was discussed in terms of blocking the electrode surface by adsorption of the molecules through the active centers contained in their structures following Langmuir adsorption isotherm. Quantum chemical method was also employed to explore the relationship between the inhibitor molecular properties and its protection efficiency. The density function theory (DFT) is used to study the structural properties of sulfa guanidine azo derivatives in aqueous phase in an attempt to understand their inhibition mechanism. The protection efficiencies of these compounds showed a certain relationship to highest occupied molecular orbital (HOMO) energy, Mulliken atomic charges and Fukui indices.

**Keywords:** Mulliken Atomic Charges, Fukui Indices, Nickel, Environmentally-Friendly Corrosion Inhibitors, Sulfa Guanidine Azo Derivatives.

\*Correspondence Author: E-mail: dr.halamahfooz@yahoo.com

## 1. INTRODUCTION

Nickel is used in many industrial processes because of its advantages, and in consumer products, including stainless steel, magnets, coinage, rechargeable batteries, electric guitar strings, and special alloys. It is also used for plating and as a green tint in glass. Nickel is pre-eminently an alloy metal, and its chief use is in nickel steels and nickel cast irons, of which there are many varieties. It is also widely used in many other alloys, such as nickel brasses, bronzes, and alloys with copper, chromium, aluminum, lead, cobalt, silver, and gold. Hydrochloric acid solutions are used for pickling, and chemical and electrochemical etching of nickel alloys. It is very important to add inhibitors to decrease the corrosion rate of nickel in such solutions. Compounds with functional groups containing hetero-atoms, which can donate lone pairs of

electrons, are found to be particularly useful as inhibitors for metal corrosion [1-6]. Also, organic substances containing polar functions with nitrogen, oxygen, and or sulfur atoms in a conjugated system and compounds with p-bonds have been reported to show good inhibiting properties [7-12]. Both features obviously can be combined within the same molecule such as drugs. Recently, the use of antibiotics and other drugs have been investigated [13-18] and their inhibition efficiencies have been linked with their heterocyclic nature. Ciprofloxacin was investigated [19] as a corrosion inhibitor for the corrosion of mild steel in acidic medium. Also, the drug amoxycillin [20] was used as a corrosion inhibitor for mild steel in 1 N hydrochloric acid solution. Generally, it has been assumed that the first stage in the action mechanism of the inhibitors in aggressive acid media is the adsorption of the inhibitors onto the metal surface. The processes of adsorption of inhibitors are influenced by the nature and distribution of charge in the molecule, the type of aggressive electrolyte, the type of interaction between

organic molecules, and the principal types of interaction between organic inhibitors and the metal surface.

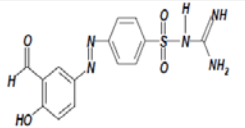
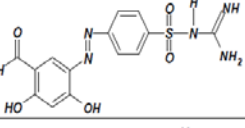
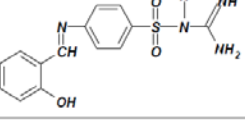
The sulfa guanidine azo derivatives which are the object of the present investigation are non-toxic, cheap and environmental friendly. They contain reactive centers like N atoms containing lone pairs of electrons and aromatic rings with delocalize  $\pi$ -electron systems which can aid their adsorption onto metal surfaces. Furthermore, they have high molecular weights and are likely to effectively cover more surface area (due to adsorption) of the metal thus preventing corrosion from taking place.

The objective of the present investigation is to study the corrosion inhibition of nickel in acidic medium using some Sulfa guanidine azo derivatives and to propose a suitable mechanism for the inhibition using the potentiodynamic polarization and ac impedance spectroscopy methods. It was also the purpose of the present work to discuss the relationship between quantum chemical calculations and experimental protection efficiencies of the three tested inhibitors by determining various quantum chemical parameters. These parameters include the highest occupied molecular orbital ( $E_{HOMO}$ ) and the lowest unoccupied molecular orbital ( $E_{LUMO}$ ), the energy difference ( $\Delta E$ ) between  $E_{HOMO}$  and  $E_{LUMO}$ .

The names, chemical and molecular structures of the investigated compounds are shown in Table (1) [21].

TABLE 1

THE NAMES, CHEMICAL AND MOLECULAR STRUCTURES OF THE INVESTIGATED COMPOUNDS

Cpd. No.	Name	Structure	Molecular Weight & Chemical Formula
(A)	Sulfa Guanidine Azo Salisaldehyde		347.0, $C_{16}H_{19}N_5O_5$
(B)	Sulfa Guanidine Azo 2,4 Dihydroxy Benzaldehyde		363.0, $C_{16}H_{19}N_5O_5$
(C)	Sulfa Guanidine Azomethine Salisaldehyde		318.0, $C_{16}H_{19}N_5O_5$

### Computational Details

Density functional theory (DFT) was used to compute of the effect some sulfa compounds on the degree of inhibition for the corrosion rate theoretically and detect the exact structure of these compounds also show the stable compound which can be used as inhibitor more than others. The effect of substitution was investigated theoretically and the excited state for all compounds was investigated by applying UV calculations to determine the

different types of electronic transition which can be occurred on these compounds with different substituent. The Frontier molecular orbitals was studied for its important role in the electric and optical properties, as well as in UV-Vis. Spectra and chemical reactions. Such computational characterization reduces time consuming experiments for biomedical and pharmaceutical studies of the drugs and its complexes. Profiles of the optimal set and geometry of these complexes were simulated by applying the GAUSSIAN 98W package of programs [22] at B3LYP/Cep-31G [23] level of theory.

## 3. EXPERIMENTAL DETAILS

### 3.1. Materials and Solutions

The chemical composition of nickel is 99.9 % BDH grade. For polarization measurements, nickel electrodes were cut from Ni wire (diameter 0.5 mm). The electrodes were of dimension 1 cm length. The samples were embedded in a glass tube. Epoxy resin was used to stick the sample to glass tube. The electrode was abraded with different grades of emery papers, degreased with acetone and rinsed by bidistilled water. All chemicals and reagents used were of analytical grade. Stock solutions (1000 ppm) of investigated sulfa guanidine azo derivatives were prepared by dissolving calculated weight of each material in one liter of bidistilled water. The measurements were carried out at 25°C using thermostatic water bath controlled to  $\pm 1$  °C.

### 3.2. Measurements

#### 3.2.1. Polarization Measurements

Potentiodynamic polarization technique was performed using a Potentiostat/ Galvanostat (Gamry PCI300) and a personal computer with DC105 software for calculations. In this method, the working electrode was immersed in the test solution for 30 min until the open potential circuit potential reached. After that the working electrode was polarized in both cathodic and anodic directions. The values of corrosion current density ( $i_{corr}$ ) were calculated from the extrapolation of Tafel lines to pre-determined open circuit potential. Standard ASTM glass electrochemical cell was used. Platinum electrode was used as auxiliary electrode. All potentials were measured against saturated calomel electrode (SCE) as a reference electrode. Polarization measurements were carried from -1200 to +200 mV with respect to corrosion potential ( $E_{corr}$ ) at a scanning rate of 1mVs-1 and % IE was determined as:

$$\% IE = [1 - (i_{corr}/i_{corr}^0)] \times 100 \quad (1)$$

Where  $i_{corr}$  and  $i_{corr}^0$  are the current densities in absence and presence of inhibitors, respectively.

### 3.2.2. Electrochemical Impedance Spectroscopy Measurements (EIS)

EIS measurements were carried out using a Potentiostat/Galvanostat (Gamry PCI300) attached with software program EIS 300. The measurements were carried out using AC signal 10 mV peak to peak at the open circuit potential in the frequency range of 100 kHz–0.5 Hz.

### 3.2.3. Electrochemical Frequency Modulation (EFM)

Electrochemical frequency modulation is a non-destructive corrosion measurement technique that can directly give values of the corrosion current without prior knowledge of Tafel constants. Like EIS, it is a small signal ac technique. Unlike EIS, however, two sine waves (at different frequencies) are applied to the cell simultaneously. Because current is a non-linear function of potential, the system responds in a non-linear way to the potential excitation.

The current response contains not only the input frequencies, but also contains frequency components which are the sum, difference, and multiples of the two input frequencies. The two frequencies may not be chosen at random. They must both be small, integer multiples of a base frequency that determines the length of the experiment. Figure (9) shows representative examples for the intermodulation spectra obtained from EFM measurements. Each spectrum is a current response as a function of frequency. The two large peaks, with amplitudes of about 100 A, are the response to the 2 Hz and 5 Hz excitation frequencies. Those peaks between 1 A and 20 A are the harmonics, sums, and differences of the two excitation frequencies. These peaks are used by the EFM140 software package to calculate the corrosion current and the Tafel constants. It is important to note that between the peaks the current response is very small. There is nearly no response (<100 nA) at 4.5 Hz, for example, the frequencies and amplitudes of the peaks are not coincidences. They are direct consequences of the EFM theory.

## 4. Results and Discussion

### 4.1. Theoretical (Computational) Study

The geometric parameters and energies were computed by density functional theory at the B3LYP/Cep-31G level of theory, using the GAUSSIAN 98W package of the programs, on geometries that were optimized at Cep-31G basis set. The high basis set was chosen to detect the energies at a highly accurate level. The atomic charges were computed using the natural atomic orbital populations. The B3LYP is the keyword for the hybrid functional [24], which is a linear combination of the gradient functionals proposed

by Becke [25] and Lee, Yang and Parr [26], together with the Hartree-Fock local exchange function [27].

### 4.1.1 Structural Parameters and Model of Sulfa Compounds

#### A- Sulfa Guanidine Azo Salisaldehyde

The activity of sulfa compounds is mainly determined by its fine structure, the sulfa guanidine azo salisaldehyde has many characteristic structural features. The molecule is a highly sterically-hindered, there are two aromatic rings. The molecule is non planer, there are two plans one occupied by the two aromatic rings and other plane occupied by the rest of molecule and also, the two plans are perpendicular respect to each other. The bond length N1-C2 is 1.339 Å, C2-N3 is 1.286 Å, there is a double bond characters C and N atoms [28], whereas C2-N4 is double bond 1.345 Å [28]. Detailed analysis of corresponding bond lengths in various sulfa molecules was given elsewhere [29]. All distances and angles between the atoms of the sulfa compound system are given in Table (2). The S5-O7 and S5-O8 bond lengths are 1.438 Å and 1.439 Å respectively, the C25-O27 bond length is 1.209 Å and N15-N16 is 1.248 Å.

The molecule is a highly sterically-hindered, the sulfa guanidine azo salisaldehyde compound occupied two plans they are perpendicular to each other. The terminal residue is out of plane of the plane occupied by the two aromatic rings, the dihedral angle N1C2N4S5, 164.10° and N3C2N4S5, -18.09°, also the dihedral angles: C2N4S5C9, 108.01°, and C2N4S5O7, -144.07°, where the values are neither zero nor 180°. Fig.(1), shows the optimized geometrical structure of sulfa guanidine azo salisaldehyde compound, the dihedral angles N15N16C17C18 is 179.82° and C12N15N16C17 is -179.07° also, O7S5C9C14, 3.44° and O7S5C9C10 is 176.23° which confirms that the N4 lying in the out of plane of the molecule.

Table (2) gives the optimized geometry of sulfa guanidine azo salisaldehyde as obtained from B3LYP/Cep-31G calculations. These data are drowning to give the optimized geometry of molecule. The value of bond angle C2N4S5 is 127.71°, O7S5O8 is 124.28°, N4S5C9 is 99.18° and C17N16N15 is 117.81° reflects on sp<sup>2</sup> hybridization, the same result is obtained with C2, the bond angle N1C2N3 is 118.99°. The values of bond distances are compared nicely with that obtained from X-ray data [28]. Comparisons of the performance of different DFT methods allow outlining the main trends of these theoretical approaches which are necessary to better understand the properties and reaction mechanisms of sulfa guanidine azo salisaldehyde compound. However, till now, no attempt has been made to analyze the application of various DFT methods and

different basis sets for accurate calculations of structure of sulfa guanidine azo salisaldehyde [29-30].

The S atom is bonded strongly with surrounded two oxygen atoms, nitrogen and carbon atom, Also the charge accumulated on S5 (1.234), O7 (-0.599) and O8 (-0.585). The charge accumulated in N1 (-0.384), N3 (-0.522) N4 (-0.436) and for azo group N15 (-0.127), N16 (-0.088). The presence of OH group effect on the charge spreading overall sulfa compound, the charge on O23 (-0.346) of -OH group and C25 (0.270), O27 (-0.308) for -CHO group. The energy of this compound is -230.019606317 au and highly dipole 7.411D

### B- Sulfa Guanidine Azo 2, 4 Dihydroxy Benzaldehyde

The activity of sulfa compounds is mainly determined by its fine structure, the sulfa guanidine azo 2, 4 dihydroxy benzaldehyde has the same characteristic structural features of sulfa guanidine azo salisaldehyde but it has -OH group in p-position respect to -CHO group in terminal aromatic ring, so we study the effect of the presence of two -OH groups and -CHO group on behavior of sulfa guanidine azo 2, 4 dihydroxy benzaldehyde and show the difference between it and sulfa guanidine azo salisaldehyde. The molecule is a highly sterically-hindered, there are two aromatic rings. The molecule is non planer, there are two plans one occupied by the two aromatic rings and other plane occupied by the rest of molecule and also, the two plans are perpendicular respect to each other. The bond length N1-C2 is 1.339Å, C2-N3 is 1.286 Å, there is a double bond characters C and N atoms [28], whereas C2-N4 is double bond 1.345Å [29]. Detailed analysis of corresponding bond lengths in various sulfa molecules was given elsewhere [29]. All distances and angles between the atoms of the sulfa compound system are given in Table (3). The S6-O7 and S6-O8 bond lengths are 1.438 Å and 1.439 Å respectively, the C27-O29 bond length is 1.209 Å and N15-N16 is 1.248 Å, for -OH groups, the C19-O23 and C21-O25 bond lengths are 1.361 Å and 1.360 Å.

The terminal residue is out of plane of the plane occupied by the two aromatic rings, the dihedral angle N1C2N4S6, -6.80° and N3C2N4S6, 174.22°, also the dihedral angles: N4S6C9C14, 112.62°, and N4S6C9C10, -67.50°, where the values are neither zero nor 180°. Fig.(3), shows the optimized geometrical structure of sulfa guanidine azo 2, 4 dihydroxy benzaldehyde compound, the dihedral angles N15N16C17C18 is -179.37° and C12N15N16C17 is 179.37° also, N16N15C12C11, -179.33° and C18C20C27O29 is 179.87° which confirms that the N4 lying in the out of plane of the molecule.

Table (3) gives the optimized geometry of sulfa guanidine azo 2, 4 dihydroxy benzaldehyde as

obtained from B3LYP/Cep-31G calculations. These data are drowning to give the optimized geometry of molecule. The value of bond angle C2N4S6 is 127.24°, O7S6O8 is 124.00°, N4S6C9 is 99.63° and C17N16N15 is 119.01° reflects on sp<sup>2</sup> hybridization, the same result is obtained with C2, the bond angle N1C2N3 is 117.99°. Comparisons of the performance of different DFT methods allow outlining the main trends of these theoretical approaches which are necessary to better understand the properties and reaction mechanisms of sulfa guanidine azo 2, 4 dihydroxy benzaldehyde compound. However, till now, no attempt has been made to analyze the application of various DFT methods and different basis sets for accurate calculations of structure of sulfa guanidine azo 2, 4 dihydroxy benzaldehyde [30-33].

The S atom is bonded strongly with surrounded two oxygen atoms, nitrogen and carbon atom, Also the charge accumulated on S6 (1.212), O7 (-0.598) and O8 (-0.602). The charge accumulated in N1 (-0.395), N3 (-0.519) N4 (-0.429) and for azo group N15 (-0.125), N16 (-0.078). The presence of two -OH groups in addition to -CHO group effect on the charge spreading overall sulfa compound, the charge on O23 (-0.329), O25 (-0.325) of -OH groups and C27 (0.269), O29 (-0.305) for -CHO group. The energy of this compound is -247.022688491 au, so that the sulfa guanidine azo 2, 4 dihydroxy benzaldehyde compound is more stable than the sulfa guanidine azo salisaldehyde which has higher energy value. The value of dipole for the sulfa guanidine azo 2, 4 dihydroxy benzaldehyde compound is 5.595D, this value attributed to the presence of -OH group in p-position respect to strong withdrawing -CHO group but in the sulfa guanidine azo salisaldehyde compound there is no -OH group in p-position respect to -CHO group so it has greater value of dipole more than the sulfa guanidine azo 2, 4 dihydroxy benzaldehyde compound.

### C- Sulfa Guanidine Azomethine Salisaldehyde

The molecule is non planer, there are two plans one occupied by the one central aromatic ring and other plane occupied by the two terminal ends of molecule and also. The bond length N1-C2 is 1.339Å, C2-N3 is 1.286 Å, there is a double bond characters C and N atoms [28], whereas C2-N5 is double bond 1.345Å [7]. All distances and angles between the atoms of the sulfa compound system are given in Table (4). The S7-O8 and S7-O9 bond lengths are 1.439 Å, the C24-O25 bond length is 1.356 Å and N16-C17 is 1.347 Å.

The molecule is less sterically-hindered, the sulfa guanidine azomethine salisaldehyde compound occupied two plans they are perpendicular to each other. The two terminal ends around the central aromatic ring is

out of plane of this ring, the dihedral angle O8S7C10C11,  $-74.81^\circ$  and N3C2N5S7,  $-176.36^\circ$ , also the dihedral angles: C2N5S7C10,  $64.64^\circ$ , and N5S7C10C11,  $39.97^\circ$ , where the values are neither zero nor  $180^\circ$ . Fig.(3), shows the optimized geometrical structure of Sulfa guanidine azomethine salisaldehyde compound, the dihedral angles N16C17C18C20 is  $179.93^\circ$  and N16C17C18C24 is  $0.39^\circ \approx 0.00$  also, C13N16C17C18,  $10.03^\circ$  and O9S7C10C11 is  $156.38^\circ$  which confirms that the N5 and C17 are lying out of the plane of the molecule.

Table (4) gives the optimized geometry of sulfa guanidine azomethine salisaldehyde as obtained from B3LYP/Cep-31G calculations. These data are drowning to give the optimized geometry of molecule. The value of bond angle C2N5S7 is  $125.68^\circ$ , O8S7O9 is  $129.54^\circ$ , N5S7C10 is  $101.55^\circ$  and C18C17N16 is  $136.32^\circ$  reflects on  $sp^2$  hybridization, the same result is obtained with C2, the bond angle N1C2N3 is  $118.72^\circ$ .

The S atom is bonded strongly with surrounded two oxygen atoms, nitrogen and carbon atom, Also the charge accumulated on S7 (1.209), O8 (-0.601) and O9 (-0.609). The charge accumulated in N1 (-0.393), N3 (-0.517) N5 (-0.429) and N16 (-0.241), C17 (0.103). There is only -OH group effect on the charge spreading overall sulfa compound, the charge on O25 (-0.351) of -OH group. The energy of this compound is  $-203.190489223$  au, this complex less stable than other two complexes because of it has energy value greater than other above studied complexes and the value of dipole is 6.74D.

#### 4.1.2. Frontier Molecular Orbitals

The frontier molecular orbitals play also an important role in the electric and optical properties, as well as in UV-Vis. Spectra and chemical reactions [34]. Fig. 4 shows the distributions and energy levels of HOMO and LUMO orbitals computed for the all sulfa compounds. For sulfa guanidine azo salisaldehyde compound the values of the energy of HOMO and LUMO are given in Table (5), the difference between HOMO and LUMO is 0.06526, for sulfa guanidine azo 2, 4 dihydroxy benzaldehyde compound the values of HOMO and LUMO are given in Table (5), the difference between HOMO and LUMO is 0.0653 and for sulfa guanidine azomethine salisaldehyde compound the values of HOMO and LUMO are given in Table (5), the difference between HOMO and LUMO is 0.10356, also the values of HOMO<sup>-1</sup>, HOMO<sup>-2</sup>, LUMO<sup>+1</sup> and LUMO<sup>+2</sup> are given in Table (5)

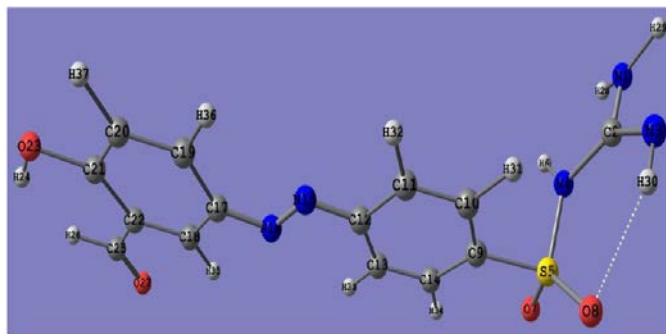


FIG. 1: THE OPTIMIZED GEOMETRICAL STRUCTURE OF SULFA GUANIDINE AZO SALISALDEHYDE COMPOUND BY USING B3LYP/CEP-31G



FIG. 2: OPTIMIZED GEOMETRICAL STRUCTURE OF SULFA GUANIDINE AZO 2, 4 DIHYDROXY BENZALDEHYDE COMPOUND BY USING B3LYP/CEP-31G

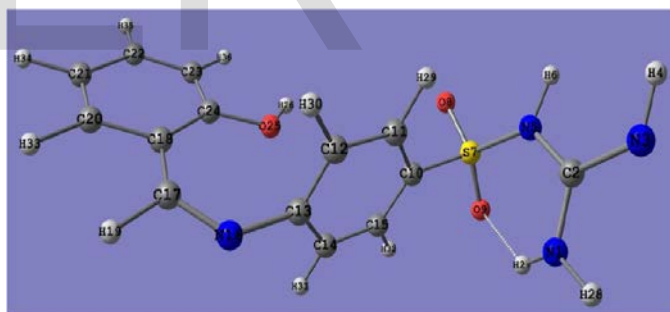
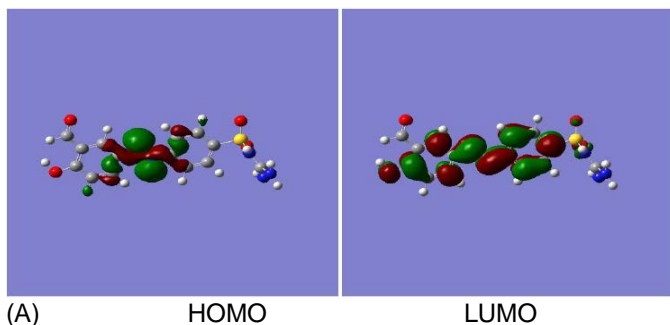


FIG. 3: OPTIMIZED GEOMETRICAL STRUCTURE OF SULFA GUANIDINE AZOMETHINE SALISALDEHYDE COMPOUND BY USING B3LYP/CEP-31G



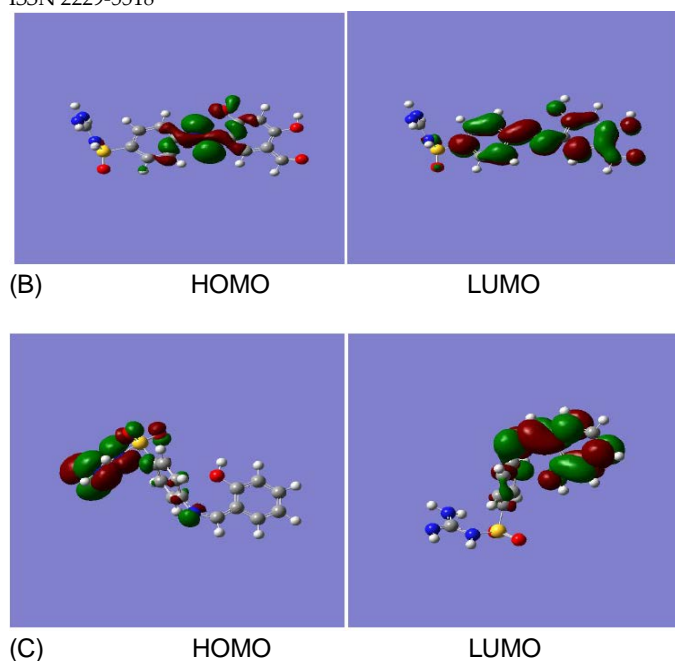


FIG. 4; MOLECULAR ORBITAL SURFACES AND ENERGY LEVELS OF (A) SULFA GUANIDINE AZO SALISALDEHYDE, (B) SULFA UANIDINE AZO 2, 4 DIHYDROXY BENZALDEHYDE AND (C) SULFA GUANIDINE AZOMETHINE SALISALDEHYDE COMPOUND BY USING B3LYP/CEP-31G.

TABLE 2  
EQUILIBRIUM GEOMETRIC PARAMETERS BOND LENGTHS (Å), BOND ANGLES (°), DIHEDRAL ANGLES (°) AND CHARGE DENSITY OF SULFA GUANIDINE AZO SALISALDEHYDE COMPOUND BY USING DFT/B3LYP/CEP-31G.

Bond Length (Å)							
N1-C2	1.339	C9-C10	1.346	N15-N16	1.248	C21-O23	1.362
C2-N3	1.286	C10-C11	1.342	N16-C17	1.266	C20-C21	1.344
C2-N4	1.345	C11-C12	1.344	C17-C18	1.345	C19-C20	1.341
N4-S5	1.636	C12-C13	1.345	C18-C22	1.346	C17-C19	1.345
S5-O7	1.438	C13-C14	1.343	C22-C25	1.359	C21-C22	1.349
S5-C9	1.745	C9-C14	1.346	C25-O27	1.209	C12-N15	1.265
S5-O8	1.439						
Bond Angle (°)							
N1C2N3	118.99	C10C9C14	117.68	C9C14C13	121.23	C12N15N16	118.33
C2N4S5	127.71	N3C2N4	125.04	C12C13C14	120.92	N16C17C19	125.39
N4S5C9	99.18	N4S5O8	113.46	C11C12C13	117.91	C17N16N15	117.81
O7S5O8	124.28	O8S5C9	100.56	C10C11C12	121.12	C18C17C19	117.87
S5C9C14	122.24	S5C9C10	120.08	C9C10C11	121.14	N16C17C18	116.73
N1C2N4	115.92	C18C22C25	118.27	C11C12N15	116.27	C17C18C22	121.33
N4S5O7	111.56	C22C21C20	116.92	C13C12N15	125.82	C18C22C21	121.08
O7S5O8	124.28	C19C20C21	122.38	C20C21O23	118.41	C22C25C27	126.19
O7S5C9	102.93	C21C22C25	120.65	C22C21C23	124.66	C17C19C20	120.42
Dihedral Angles (°)							
C2N4S5O7	-144.07	C2N4S5O8	2.19	O8S5C9C14	-125.67		
N1C2N4S5	164.10	O8S5C9C10	54.67	C12N15N16C17	-179.07		
N4S5C9C14	118.21	O7S5C9C14	3.44	N15N16C17C18	179.82		
O7S5C9C10	-176.23	N15N16C17C19	0.00	N4S5C9C10	-61.45		
N3C2N4S5	-18.09	C2N4S5C9	108.01				
Charges							
N1	-0.384	O8	-0.585	C14	0.006	C20	-0.09
C2	0.466	C9	-0.069	N15	-0.127	C21	0.249
N3	-0.522	C10	0.003	N16	-0.088	C22	-0.077
N4	-0.436	C11	-0.068	C17	0.123	O23	-0.346
S5	1.234	C12	0.182	C18	-0.019	C25	0.27
O7	-0.599	C13	-0.074	C19	-0.021	O27	-0.308
Total Energy/au				-230.019606317			
Total Dipole Moment/D				7.411			



TABLE 3

EQUILIBRIUM GEOMETRIC PARAMETERS BOND LENGTHS (Å), BOND ANGLES (°), DIHEDRAL ANGLES (°) AND CHARGE DENSITY OF SULFA GUANIDINE AZO 2, 4 DIHYDROXY BENZALDEHYDE COMPOUND BY USING DFT/B3LYP/CEP-31G.

Bond Length (Å)								
N1-C2	1.339	C9-C10	1.346	C20-C21	1.345	C11-C12	1.344	
C2-N3	1.286	C13-C14	1.343	C21-C22	1.344	C12-N15	1.265	
C2-N4	1.345	C17-N16	1.266	C10-C11	1.342	C18-C20	1.345	
N4-S6	1.637	C20-C27	1.359	C9-C14	1.346	C21-O25	1.360	
S6-O7	1.438	C19-C22	1.349	C17-C18	1.346	C19-O23	1.361	
S6-O8	1.439	C12-C13	1.345	C27-O29	1.209			
S6-C9	1.756	N15-N16	1.248	C17-C19	1.349			
Bond Angle (°)								
N1C2N3	117.99	C9S6O8	100.66	N16C17C19	125.87	C20C21O25	122.88	
N3C2N4	118.42	S6C9C10	120.22	C18C17C19	119.25	C21C22C19	123.67	
N1C2N4	123.59	S6C9C14	122.14	C17C18C20	121.21	C17C19O23	122.49	
C2N4S6	127.24	C9C10C11	121.18	C18C20C21	120.59	C22C19O23	119.32	
N4S6C9	99.63	C10C11C12	121.09	C18C20C27	119.21	N16C17C18	114.88	
N4S6O7	111.48	C11C12C13	117.89	C21C20C27	120.19	N15N16C17	119.01	
N4S6O8	113.56	C12C13C14	120.94	C22C21O25	120.05	C20C21C22	117.08	
O7S6O8	124.00	C9C14C13	121.25	C17C19C22	118.19	C12N15N16	118.34	
O7S6C9	102.86	C13C12N15	125.73	C20C27O29	127.23	C11C12N15	116.37	
Dihedral Angles (°)								
N3C2N4S6	174.22	N1C2N4S6	-6.8	N4S6C9C10	-67.50			
N4S6C9C14	112.62	O7S6C9C14	-2.19	O7S6C9C10	177.68			
C10C9S6O8	48.88	C14C9S6O8	-130.99	C12N15N16C17	179.37			
N15N16C17C18	-179.37	N16N15C12C11	-179.33	C18C20C27O29	179.87			
Charges								
N1	-0.395	C9	-0.07	N16	-0.078	O23	-0.329	
C2	0.47	C10	0.004	C17	0.064	O25	-0.325	
N3	-0.519	C11	-0.069	C18	-0.009	C27	0.269	
N4	-0.429	C12	0.184	C19	0.248	O29	-0.305	
S6	1.212	C13	-0.077	C20	-0.085			
O7	-0.598	C14	0.007	C21	0.287			
O8	-0.602	N15	-0.125	C22	-0.202			
Total Energy/au					-247.022688491			
Total Dipole Moment/D					5.595			

TABLE 4

EQUILIBRIUM GEOMETRIC PARAMETERS BOND LENGTHS (Å), BOND ANGLES (°), DIHEDRAL ANGLES (°) AND CHARGE DENSITY OF SULFA GUANIDINE AZOMETHINE SALISALDEHYDE COMPOUND BY USING DFT/B3LYP/CEP-31G.

Bond Length (Å)								
N1-C2	1.339	C10-C11	1.347	N16-C17	1.347	C18-C24	1.352	
C2-N3	1.286	C11-C12	1.342	C1-7C18	1.349	C24-O25	1.356	
C2-N5	1.345	C12-C13	1.342	C18-C20	1.352	C23-C24	1.346	
N5-S7	1.635	C13-C14	1.342	C20-C21	1.341	C13-N16	1.344	
S7-O8	1.439	C14-C15	1.343	C21-C22	1.338	S7-C10	1.744	
S7-O9	1.439	C10-C15	1.347	C22-C23	1.339			
Bond Angle (°)								
N1C2N3	118.72	S7C10C11	120.31	N16C17C18	136.32	C17C18C24	127.55	
N1C2N5	122.25	S7C10C15	121.25	C18C20C21	122.71	C21C22C23	118.65	
N3C2N5	119.01	C11C10C15	118.43	C22C23C24	122.41	C23C24O25	117.24	
C2N5S7	125.68	C10C15C14	120.96	C18C24O25	123.38	C13N16C17	125.49	
N5S7O8	111.83	C15C14C13	119.8	C14C13N16	119.94	C12C13N16	120.04	
N5S7O9	112.41	C14C13C12	120.01	C17C18C20	114.94	O9S7C10	102.65	
O8S7O9	129.54	C11C12C13	119.75	C20C21C22	119.34			
O8S7C10	99.52	C10C11C12	121.04	C18C24C23	119.38			
Dihedral Angles (°)								
N1C2N5S7	1.66	N3C2N5S7	-176.36	C2N5S7C10	64.64			
N5S7C10C11	39.97	N5S7C10C15	-141.31	O8S7C10C11	-74.81			
O8S7C10C15	103.91	O9S7C10C15	-24.89	O9S7C10C11	156.38			
C13N10C17C18	10.03	C17N16C13C12	78.26	C17N16C13C14	-102.65			
N16C17C18C24	0.39	N16C17C18C20	179.93					
Charges								
N1	-0.393	O9	-0.609	C15	0.021	C22	0.019	
C2	0.469	C10	-0.089	N16	-0.241	C23	-0.112	
N3	-0.517	C11	0.016	C17	0.103	C24	-0.351	
N5	-0.429	C12	-0.089	C18	-0.024	O25	-0.351	
S7	1.209	C13	0.222	C20	-0.003			
O8	-0.601	C14	-0.089	C21	-0.055			
Total Energy/au					-203.190489223			
Total Dipole Moment/D					6.74			

TABLE 5

VALUES OF ENERGY (EV) OF HOMO AND LUMO FOR THE (A) SULFA GUANIDINE AZO SALISALDEHYDE, (B) SULFA GUANIDINE AZO 2, 4 DIHYDROXY BENZALDEHYDE AND (C) SULFA GUANIDINE AZOMETHINE SALISALDEHYDE COMPOUND BY USING

B3LYP/CEP-31G.			
	(A)	(B)	(C)
LUMO <sup>2</sup>	-0.14683	-0.14689	-0.13833
LUMO <sup>1</sup>	-0.18683	-0.16816	-0.14759
<b>LUMO</b>	<b>-0.21293</b>	<b>-0.207</b>	<b>-0.19344</b>
<b>HOMO</b>	<b>-0.27819</b>	<b>-0.2723</b>	<b>-0.297</b>
HOMO <sup>1</sup>	-0.29911	-0.29625	-0.30833
HOMO <sup>2</sup>	-0.30047	-0.29731	-0.31257
$\Delta E = \text{HOMO} - \text{LUMO}$	<b>0.06526</b>	<b>0.0653</b>	<b>0.10356</b>

## 4.2. Experimental Study

### 4.2.1. Potentiodynamic Polarization Technique

Figure (5) shows typical anodic and cathodic Tafel polarization curves for nickel in 0.5 M HCl in the absence and presence of varying concentrations of compound (A) at 25 °C.. Similar curves were obtained for the other compounds (not shown). As reflected from the graph, the additive exhibits a significant effect on the corrosion current density ( $i_{corr}$ ) and the corrosion potential ( $E_{corr}$ ) values. Table (6) shows the effect of the inhibitor concentration on the corrosion kinetics parameters, such as Tafel slopes ( $\beta_a$ ,  $\beta_c$ ), corrosion potential ( $E_{corr}$ ), corrosion current density ( $i_{corr}$ ) and inhibition efficiency (% IE). The results of Table (6) indicate that, the Tafel lines are shifted to more negative and more positive potentials for the cathodic and the anodic processes, respectively, relative to the uninhibited (Blank) curve. This means that these additives influence both the cathodic and the anodic processes and the process of inhibition is believed to be mixed inhibition process, i.e., the inhibitors are of mixed types. It is also, observed that the presence of these additives doesn't shift  $E_{corr}$  remarkably, therefore, these additives could be regarded as mixed-type inhibitors and their inhibition on Ni surface occurred by blocking effect mechanism [35]. The slopes of the cathodic and anodic Tafel lines are approximately constant and independent on the inhibitor concentration. This behavior suggests that the inhibitor molecules have no effect on the metal dissolution mechanism. A decrease in the corrosion current density ( $i_{corr}$ ) was observed by increasing the concentration of the inhibitor used. The order of % IE obtained from polarization measurements is as follows: A > B > C.

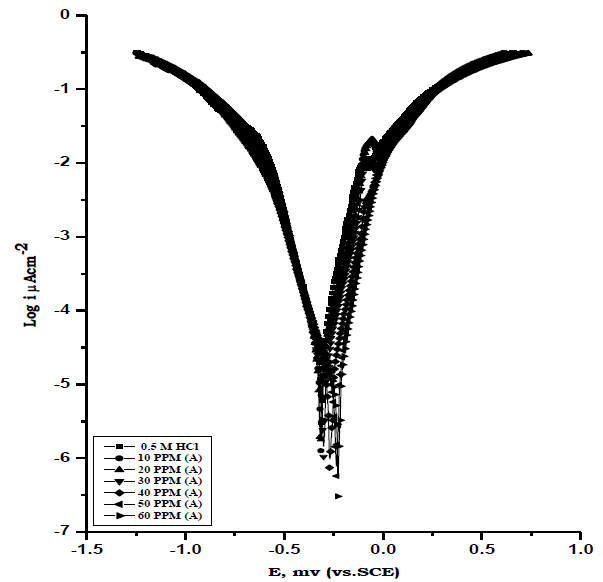


FIG. 5: POTENTIODYNAMIC POLARIZATION CURVES FOR NICKEL IN 0.5 M HCL IN THE ABSENCE AND PRESENCE OF DIFFERENT CONCENTRATIONS OF COMPOUND (A) AT 25 °C

TABLE 5  
VALUES OF ENERGY (EV) OF HOMO AND LUMO FOR THE (A) SULFA GUANIDINE AZO SALISALDEHYDE, (B) SULFA GUANIDINE AZO 2, 4 DIHYDROXY BENZALDEHYDE AND (C) SULFA GUANIDINE AZOMETHINE SALISALDEHYDE COMPOUND BY USING 3LYP/CEP-31G.

	(A)	(B)	(C)
LUMO <sup>2</sup>	-0.14683	-0.14689	-0.13833
LUMO <sup>1</sup>	-0.18683	-0.16816	-0.14759
<b>LUMO</b>	<b>-0.21293</b>	<b>-0.207</b>	<b>-0.19344</b>
<b>HOMO</b>	<b>-0.27819</b>	<b>-0.2723</b>	<b>-0.297</b>
HOMO <sup>1</sup>	-0.29911	-0.29625	-0.30833
HOMO <sup>2</sup>	-0.30047	-0.29731	-0.31257
$\Delta E = \text{HOMO} - \text{LUMO}$	<b>0.06526</b>	<b>0.0653</b>	<b>0.10356</b>

TABLE 6  
THE EFFECT OF INHIBITOR CONCENTRATION ON THE FREE CORROSION POTENTIAL ( $E_{corr}$ ), CORROSION CURRENT DENSITY ( $i_{corr}$ ), TAFEL SLOPES ( $\beta_a$  &  $\beta_c$ ), INHIBITION

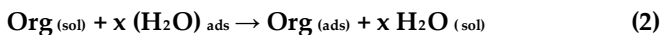


## EFFICIENCY (% IE), AND CORROSION RATE FOR THE CORROSION OF NICKEL IN 0.5 M HCl AT 25 °C

Conc. ppm		$E_{corr}$ , mV vs.SCE	$i_{corr}$ , $\mu\text{A cm}^{-2}$	$\beta_a$ , mV dec <sup>-1</sup>	$\beta_c$ , mV dec <sup>-1</sup>	$\theta$	% IE
0.0		312	14.90	263	287	---	---
Compound (A)	10	239	3.12	243	254	0.790	79.0
	20	265	2.85	237	245	0.808	80.8
	30	290	2.49	219	234	0.832	83.2
	40	295	1.79	212	231	0.879	87.9
	50	253	1.06	211	178	0.928	92.8
	60	274	1.03	204	176	0.930	93.0
Compound (B)	10	293	3.91	216	217	0.737	73.7
	20	238	3.47	221	227	0.767	76.7
	30	285	2.97	203	211	0.800	80.0
	40	179	2.74	242	237	0.816	81.6
	50	281	2.32	169	188	0.844	84.4
	60	273	2.08	166	192	0.860	86.0
Compound (C)	10	314	8.89	253	244	0.403	40.3
	20	319	7.44	248	243	0.500	50.0
	30	305	5.81	235	366	0.610	61.0
	40	267	3.64	215	219	0.755	75.5
	50	238	2.65	221	234	0.822	82.2
	60	226	2.33	212	223	0.843	84.3

## 4.2.2. Adsorption Isotherm

The adsorption of the inhibitors is influenced by the nature and charge of the metal, the chemical structure of the inhibitors, distribution of the charge in the molecule, and the type of electrolyte [36-38]. Important information about the interaction between the inhibitor and nickel surface can be obtained by the adsorption isotherm. The values of surface coverage,  $\theta$ , increase with the inhibitor concentration, this is attributed to more adsorption of inhibitors onto the nickel surface. The adsorption of organic adsorbate on the surface of nickel electrode is regarded as substitutional adsorption process between the organic compound in the aqueous phase ( $\text{Org}_{aq}$ ) and the  $\text{H}_2\text{O}$  molecules adsorbed on the Nickel surface ( $\text{H}_2\text{O}_{ads}$ ) [39].



Where  $x$  is the size ratio, that is, the number of  $\text{H}_2\text{O}$  molecules replaced by one organic molecule.

Attempts were made to fit  $\theta$  values to various isotherms including Frumkin, Langmuir, Temkin and Freundlich isotherms. By far the results were best fitted by Langmuir adsorption isotherm which has the following equation:

$$C/\theta = 1/K + C \quad (3)$$

Where  $C$  is the inhibitor concentration in the electrolyte and  $K$  is the equilibrium constant for the adsorption/desorption process. The value of  $K$  is related to the free energy of adsorption,  $\Delta G^\circ_{ads}$ , by the equation:

$$K = 1/55.5 \exp (\Delta G^\circ_{ads}/RT) \quad (4)$$

Where  $R$  is the universal gas constant,  $T$  is the absolute temperature and 55.5 is the concentration of water in bulk solution in  $\text{M}^{-1}$ . The high value of  $K$  (Table 7) reflects the high adsorption ability of these sulfa guanidine azo derivatives on Ni surface. The value of  $K$  was found to be in the order:  $A > B > C$  which is runs parallel to the inhibition efficiency. Plotting  $\log C/\theta$  against  $\log C$  gives a straight line with approximate unit slope value (Fig. 6), indicating that the adsorption of Sulfa guanidine azo derivatives (A- C) on nickel surface follows Langmuir adsorption isotherm and hence, there is no interaction between the adsorbed species. This deviation from unity is due to, The Langmuir isotherm, originally derived for the adsorption of gas molecules on solid surfaces, was modified to fit the adsorption isotherm of solutes onto solid surfaces in solution. A modified Langmuir adsorption isotherm [40] could be applied to this phenomenon, which is given by the corrected equation:

$$C/\theta = n/K + nC \quad (5)$$

Where  $n$  is the value of slopes obtained from the plot in Fig. 6. The aim of modification was based on the fact that direct application of the Langmuir isotherm to solution systems often leads to poor data fitting [41]. The negative value of  $\Delta G^\circ_{ads}$  (Table 7) indicates spontaneous adsorption of investigated compounds on Ni surface and also the strong interaction between inhibitor molecules and the metal surface [42]. Generally, the standard free energy values of  $-20 \text{ kJ mol}^{-1}$  or less negative are associated with an electrostatic interaction between charged molecules and charged metal surface (physical adsorption), those of  $-40 \text{ kJ mol}^{-1}$  or more negative involves charge sharing or transfer from the inhibitor molecules to the metal surface to form a co-ordinate covalent bond (chemical adsorption) [43]. The calculated standard free energy of adsorption values are less than  $10 \text{ kJ mol}^{-1}$ . Therefore, it can be concluded that these compounds are adsorbed on Ni surface physically [44].

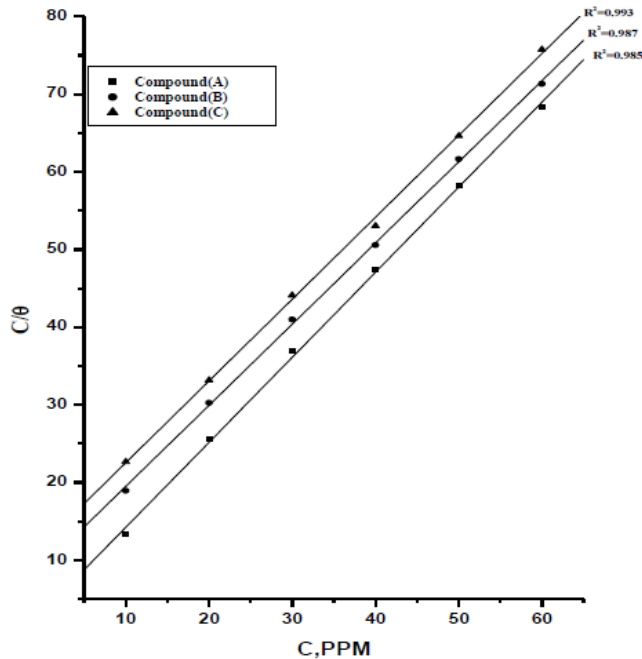


FIG. 6: CURVE FITTING OF CORROSION DATA OBTAINED FROM POTENTIODYNAMIC POLARIZATION METHOD FOR NICKEL IN 0.5 M HCL IN THE PRESENCE OF DIFFERENT CONCENTRATIONS OF INVESTIGATED COMPOUNDS TO LANGMUIR ADSORPTION ISOTHERM AT 25 °C

TABLE 7

INHIBITOR BINDING CONSTANT (K), FREE ENERGY OF BINDING ( $\Delta G_{ads}^0$ ), FOR THE INVESTIGATED SULFA GUANIDINE AZO DERIVATIVES FOR THE CORROSION OF NICKEL IN 1M HCL AT 25 °C

Sulfa Guanidine Azo Derivatives	Langmuir Adsorption Isotherm	
	$K \times 10^4 \text{ M}^{-1}$	$-\Delta G_{ads}^0, \text{ kJ mol}^{-1}$
(A)	2.8	6.9
(B)	1.9	5.7
(C)	0.89	3.9

#### 4.2.3. AC Impedance Technique

The corrosion behavior of nickel in 0.5 M HCl solution in the absence and presence of different concentrations of the sulfa guanidine azo derivatives was investigated by the EIS method at the open circuit potential conditions at 25 °C. Figure (7) shows the Nyquist plots for nickel in 0.5 M HCl solution in the absence and presence of different concentrations of compound (A) at 25 °C., respectively. Similar curves were obtained for other inhibitors (not shown). The Nyquist diagram obtained with 0.5 M HCl shows only one capacitive loop, both in uninhibited and inhibited solutions and the diameter of the semicircle increases on increasing the inhibitor concentration suggesting that the formed inhibitive film was strengthened by the addition of inhibitors. The the main

parameters deduced from the impedance technique are given in Table (8). The impedance data of nickel in 0.5 M HCl are analyzed in terms of an equivalent circuit model Figure (8) which includes the solution resistance  $R_s$  or  $R_\Omega$  and the double layer capacitance  $C_{dl}$  which is placed in parallel to the charge transfer resistance  $R_{ct}$  due to the charge transfer reaction [45].

$$C_{dl} = (1 / 2\pi f_{max} R_{ct}) \quad (6)$$

Where  $f_{max}$  is the maximum frequency. The inhibition efficiencies and the surface coverage ( $\theta$ ) obtained from the impedance measurements are defined by the following relations:

$$\% \text{ IE} = [1 - (R_{ct} / R_{ct}^0)] \times 100 \quad (7)$$

$$\theta = [1 - (R_{ct}^0 / R_{ct})] \quad (8)$$

Where  $R_{ct}^0$  and  $R_{ct}$  are the charge transfer resistance in the absence and presence of inhibitor, respectively. From the impedance data given in Table (8), we conclude that: The value of  $R_{ct}$  increases with increasing the concentration of the inhibitors indicating the decreased corrosion rate (i.e. increased corrosion inhibition) in acidic solution. As the impedance diagram obtained has a semicircle appearance, it shows that the corrosion of nickel is mainly controlled by a charge transfer process. The value of double layer capacitance ( $C_{dl}$ ) decreases by increasing the inhibitor concentration indicating the reduction of charges accumulated in the double layer due to the formation of adsorbed inhibitor layer and its lower values indicate the inhomogeneity of surface of the metal roughened due to corrosion [46]. The inhibition efficiencies calculated according to the impedance results are in the order:  $A > B > C$  and these results follow the same trend as the polarization results. The % IE obtained from EIS measurements are close to those deduced from potentiodynamic polarization method.

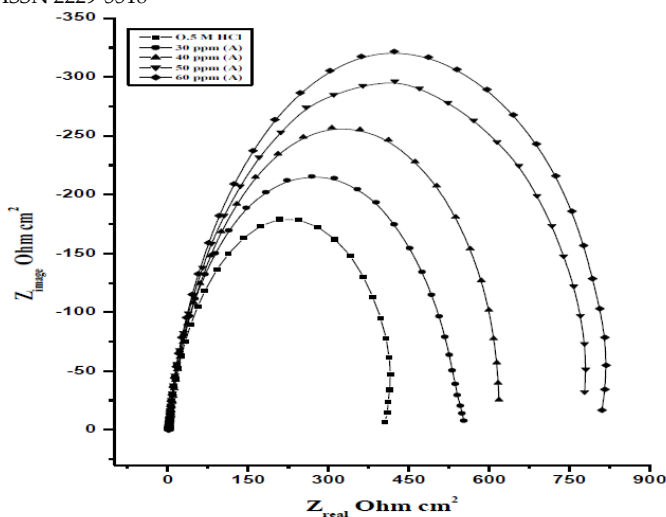


FIG. 7: THE NYQUIST PLOTS FOR NICKEL IN 0.5 M HCL SOLUTION IN THE ABSENCE AND PRESENCE OF DIFFERENT CONCENTRATIONS OF COMPOUND (A) AT 25 °C.

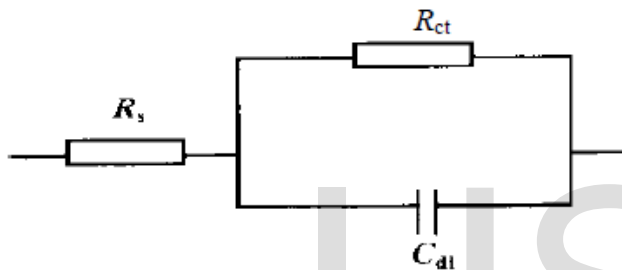


FIG. 8: EQUIVALENT CIRCUIT MODEL FITS THE IMPEDANCE DATA

TABLE 8

ELECTROCHEMICAL KINETIC PARAMETERS OBTAINED BY EIS TECHNIQUE FOR CORROSION OF NICKEL IN 0.5 M HCL AT DIFFERENT CONCENTRATIONS OF INVESTIGATED COMPOUNDS AT 25 °C

Compounds	Conc., ppm	$C_{dl}$ , $\mu F\ cm^{-2}$	$R_s$ , $\text{ohm}\ cm^2$	$\theta$	%IE
Blank	0.0	39.86	371.0	-	-
Compound (A)	30	33.99	879.0	0.577	57.7
	40	29.60	1050.0	0.646	46.6
	50	23.70	1327.1	0.720	72.0
	60	19.00	1536.0	0.758	75.8
Compound (B)	30	37.60	609.0	0.398	39.8
	40	31.50	650.0	0.429	42.9
	50	29.01	912.1	0.593	59.3
	60	31.63	1069.0	0.652	65.2
Compound (C)	30	34.30	480.3	0.227	22.7
	40	32.60	533.4	0.304	30.4
	50	33.00	656.5	0.434	43.4
	60	31.80	710.0	0.477	47.7

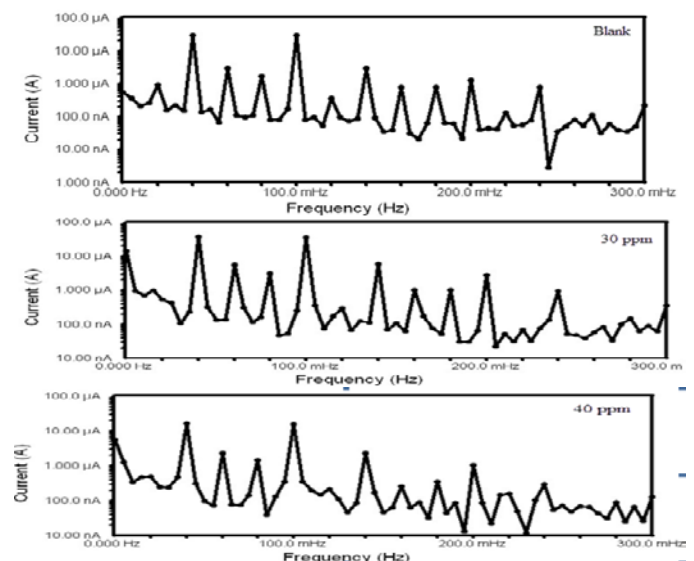
#### 4.2.4. Electrochemical Frequency Modulation (EFM) Technique

The EFM technique is used to calculate the anodic and cathodic Tafel slopes as well as corrosion current

densities for the system Ni / HCl without and with various concentrations of compound (A) at 25 °C. Figure (9) are examples representing the EFM intermodulation spectra (spectra of current response as a function of frequency) of nickel in aerated 0.5 M HCl solutions. Similar results were recorded for the other concentrations. The inhibition efficiency, % IE, of compound (A) was calculated at different concentrations using equation presented elsewhere [47].

$$\% E_{EFM} = [1 - (i_{corr} / i_{corr}^0)] \times 100 \quad (9)$$

Where  $i_{corr}$  and  $i_{corr}^0$  are the current densities in absence and presence of inhibitors, respectively. The calculated electrochemical parameters  $j_{corr}$ , CF-2, CF-3 and % IE are given in Table (9). Inspections of these data infer that the values of causality factors obtained under different experimental conditions are approximately equal the theoretical values (2) and (3) indicating that the measured data are of high quality [48]. In absence of the inhibitors (Blank) it seen that the value of corrosion current density ( $i_{corr}$ ), and hence the rate of corrosion. Addition of increasing concentration of compound (A) to HCl solution decreases the corrosion current density ( $i_{corr}$ ) at a given temperature, indicating that compound (A) inhibits the acid corrosion of nickel through adsorption. However at a given inhibitor concentration, the corrosion current density ( $i_{corr}$ ) still increases with increasing the temperature as a result of increasing the rate of corrosion and partial adsorption of inhibitor species on the nickel surface. The calculated inhibition efficiency, % IE enhances with compound (A) concentration. The inhibition efficiencies calculated according to the EFM results are in the order: A > B > C and these results follow the same trend as the polarization and impedance results.



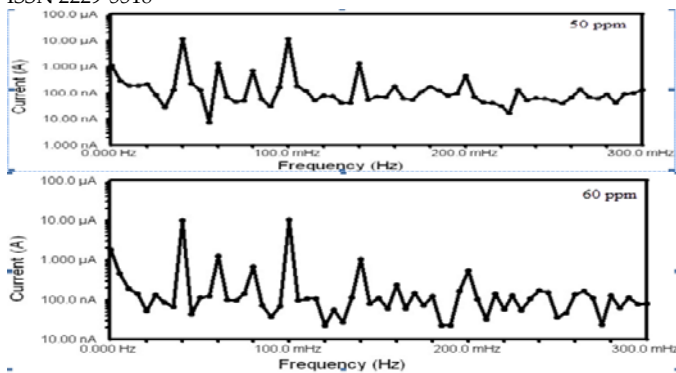


FIG. 9: EFM SPECTRA NICKEL IN 0.5M HCL IN THE ABSENCE AND PRESENCE OF DIFFERENT CONCENTRATIONS OF COMPOUND (A) AT 25°C

TABLE 9

ELECTROCHEMICAL KINETIC PARAMETERS OBTAINED FROM EFM TECHNIQUE FOR THE CORROSION OF NICKEL ELECTRODE IN 0.5 M HCL AT DIFFERENT CONCENTRATIONS OF INVESTIGATED INHIBITORS AT 25°C.

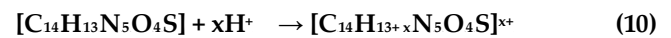
Compounds	Conc. Ppm.	$i_{cor}$ , $\mu A$ $cm^{-2}$	$\beta_c$ , mV $dec^{-1}$	$\beta_a$ , mV $dec^{-1}$	CF(2)	CF(3)	$\theta$	% IE
Blank	0.0	53.2	282	273	1.97	3.02	----	----
Compound (A)	30	24.22	255	243	1.99	3.12	0.544	54.4
	40	19.03	255	233	2.01	2.89	0.642	64.2
	50	15.90	232	222	2.00	2.88	0.701	70.1
	60	13.20	236	252	1.87	2.96	0.751	75.1
Compound (B)	30	32.76	199	219	2.04	2.87	0.384	38.4
	40	23.90	165	238	1.76	2.68	0.550	55.0
	50	21.88	242	200	2.11	2.83	0.588	58.8
	60	19.20	224	265	1.79	2.91	0.639	63.9
Compound (C)	30	41.50	213	227	2.03	2.49	0.219	21.9
	40	35.98	236	251	2.04	2.77	0.323	32.3
	50	34.01	182	180	2.12	2.88	0.360	36.0
	60	30.23	176	162	1.70	2.76	0.431	43.1

### 5. Molecular Structure Effect

It is generally assumed that adsorption at the metal/solution interface is the first step in the inhibition mechanism in aggressive acidic media, which as most organic compounds contain at least one polar group with an atom of nitrogen, sulfur or oxygen, each might be a chemisorptions center. The inhibitive action depends on the electron densities around the adsorption center; the higher the electron density at the center, the more efficient is the inhibitor. Inhibition efficiency depends on several factors

such as the number of adsorption sites and their charge density, molecular size, heat of hydrogenation, mode of interaction with the metal surface, and extent of the formation of metallic complexes [49]. The order of inhibition efficiency obtained from electrochemical measurements is as follows: A > B > C

The adsorption of these inhibitors at the Ni surface can take place through their active centers, N, O and S atoms, in addition to a  $\pi$  electron interaction of the benzene ring nucleus with unshared d electrons of Ni atoms [50-53]. The adsorption and the inhibition effect of investigated inhibitors in 0.5 M HCl solution can be explained as follows: inhibitor molecules might be protonated in the acid solution (compound A as example) as:



In aqueous acidic solutions, these inhibitors exist either as neutral molecules or as protonated molecules (cations). These inhibitors may adsorb on the metal/acid solution interface [54] by one and/or more of the following ways: (1) electrostatic attraction between charged molecules and charged metal, (2) interaction of unshared electron pairs in the molecule with the metal, (3) interaction of  $\pi$  electrons with the metal, and (4) a combination of the previous three. In general, two modes of adsorption are considered on the metal surface in acid media. In one mode, the neutral molecules may be adsorbed on the surface of the Ni via a chemisorption mechanism, involving the displacement of water molecules from the nickel surface and the sharing of electrons between the hetero-atoms and the nickel. The inhibitor molecules can also adsorb on the Ni surface on the basis of donor-acceptor interactions between p-electrons of the aromatic ring and vacant d-orbitals of surface nickel atom. In the second mode, since it is well known that the nickel surface bears a positive charge in acid solution [55], it is difficult for the protonated molecules to approach the positively charged nickel surface due to the electrostatic repulsion. Since chloride ions have a smaller degree of hydration, so they could bring excess negative charges in the vicinity of the interface and favor more adsorption of the positively charged inhibitor molecules, with the protonated inhibitors adsorbing via electrostatic interactions between the positively charged molecules and negatively charged metal surface. Thus, there is a synergism between adsorbed  $Cl^-$  ions and protonated inhibitors, and we can also conclude that inhibition of nickel corrosion in 0.5 M HCl is mainly due to electrostatic interaction. The decrease in inhibition efficiency with a rise in temperature supports electrostatic interaction. In organic compounds differing in the functional donor atom (other factors being equal), the order of corrosion inhibition is

usually:  $S > N > O$ , which is the reverse order of electronegativity. Sulfur compounds are better corrosion inhibitors than their nitrogen analogues because the S-atom, being less electronegative than N, draws fewer electrons to itself, and is thus the more efficient electron donor in forming the chemisorptive bond.

Compound (A) is the most efficient one, which is due to the presence of 1S, 5 N, and 4 O atoms in its structure, but compound (B) comes after compound (A) in inhibition efficiency. Compound (C) comes after compound (B) in inhibition efficiency. This is due to the smaller number of nitrogen atoms (4 N atoms) in its structure.

The bond gap energy  $\Delta E$  increases from (A to C). This fact explains the decreasing inhibition efficiency in this order ( $A > B > C$ ), as shown in Table (5) and Fig (4) show the optimized structures of the three investigated compounds. So, the calculated energy gaps show reasonably good correlation with the efficiency of corrosion inhibition. Table (5) also indicates that compound (A) possesses the lowest total energy that means that compound (A) adsorption occurs easily and is favored by the highest softness. The HOMO and LUMO electronic density distributions of these molecules were plotted in Fig (4). For the HOMO of the studied compounds that the benzene ring, N-atoms and O-atom have a large electron density.

## 6. Conclusions

The sulfa guanidine azo derivatives show good corrosion inhibition property against nickel corrosion in 0.5 M HCl solution. Inhibition efficiencies are related to concentration and chemical structure of the investigated derivatives. Generally, inhibition efficiencies increase when concentration increases. All investigated compounds affected both anodic and cathodic reactions, so they are classified as mixed type inhibitors. Adsorption of these derivatives on the nickel surface obeys Langmuir adsorption isotherm. EIS measurements clarified that the corrosion process was mainly charge transfer controlled and no charge in the corrosion mechanism occurred due to the inhibitor addition to acidic solutions. The bond gap energy  $\Delta E$  increases from (A to C). This fact explains the decreasing inhibition efficiency in this order ( $A > B > C$ ). So, the calculated energy gaps show reasonably good correlation with the efficiency of corrosion inhibition.

## 7. References

- [1] S.A. Umoren, I.B. Obot, *Surf. Rev. Lett.* 15(3), 277, 2008.
- [2] E.E. Ebenso, H. Alemu, S.A. Umoren, I.B. Obot. *Int. J. Electrochem. Sci.* 3, 1325, 2008.
- [3] H. Ju, Y. Li, *Corros. Sci.* 49, 4185, 2007.
- [4] G.Y. Elewady, I.A. El-Said, A.S. Fouda. *Int. J. Electrochem. Sci.* 3, 644, 2008.
- [5] W. Li, G. He, C. Pei, B. Hou. *Electrochim. Acta* 52, 6386, 2007.
- [6] M. Bouklah, B. Hammouti, M. Lagrenee, F. Bentiss. *Corros. Sci.* 48, 2831, 2006.
- [7] M. Benabdellah, R. Touzani, A. Aouniti, A. Dafali, S. El-Kadiri, B. Hammouti, M. Benkaddour. *Mater. Chem. Phys.* 105, 373, 2007.
- [8] A. Yildirim, M. Cetin. *Corros. Sci.* 50, 155, 2008.
- [9] Y. Harek, L. Larabi. *Kem. Ind.* 53(2), 55, 2004.
- [10] A. Fiala, A. Chibani, A. Darchen, A. Boulkamh, K. Djebbar. *Appl. Surf. Sci.* 253, 9347, 2007.
- [11] R. Hasanov, M. Sadikoglu, S. Bilgic. *Appl. Surf. Sci.* 253, 3913, 2007.
- [12] S.A. Umoren, O. Ogbobe, E.E. Ebenso. *Bull. Electrochem.* 22(4), 155, 2006.
- [13] M. Abdallah. *Electrochim. Acta* 22, 161, 2004.
- [14] M. Abdallah. *Corros. Sci.* A 46, 1981, 2004.
- [15] O.K. Abiola, N.C. Oforika, E.E. Ebenso. *JCSE* 5(10), 1, 2004.
- [16] N.O. Eddy, A.S. Ekop. *J. Mater. Sci.* 4(1), 10, 2008.
- [17] N.O. Eddy, S.A. Odoemelam. *J. Surf. Sci. Technol.* 24(1-2), 1, 2008.
- [18] N.O. Eddy, S.A. Odoemelam. *J. Mater. Sci.* 4, 87, 2008.
- [19] L. Magaji, P.O. Ameh, N.O. Eddy, A. Uzairu, A.A. Siaka, S. Habib, A.M. Ayuba, S.M. Gumel. *Int. J. Mod. Chem.* 2(2), 64, 2012.
- [20] S. Hari Kumar, S. Karthikeyan, S. Narayanan, K.N. Srinivasan. *Int. J. ChemTech. Res.* 4(3), 1077, 2012.
- [21] I. Sheikhsaie, M. Hossein, Mashhadizadeh, and S. Saeid-Nia. *J. Coordination Chemistry.* 57(5), 417, 2004.
- [22] **Gaussian 98**, Revision A.6, M. J. Frisch, G. W. Trucks, H. B. Schlegel, G. E. Scuseria, M.A.Robb, J.R.Cheeseman, V.G. Zakrzewski, J.A. Montgomery, Jr.,R.E.Stratman J.C.Burant, S.Dapprich, J.M.Millam, A.D.Daniels, K.N. Kudin, M.C. Strain, O. Farkas, J. Tomasi, V. Barone, M. Cossi, R. Cammi, B.Mennucci, C. Pomelli, C. Adamo, S.Clifford, J. Ochterski, G. A. Petersson, P. Y. Ayala, Q. Cui, K. Morokuma, D. K.Malick, A.D.Rabuck, K. Raghavachari, J.B. Foresman, J.Cioslowski, J.V.Ortiz, B.B.Stefanov, G.Liu, A.Liashenko, P.Piskorz, I. Komaromi, R.Gomperts,R. L. Martin, D. J. Fox, T. Keith, M. A. Al-Laham, C. Y. Peng, A. Nanayakkara, C. Gonzalez, M. Challacombe, P. M. W. Gill, B. Johnson, W. Chen, M. W. Wong, J. L.Andres, C. Gonzalez, M. Head-Gordon, E. S. Replogle, and J. A. Pople, Gaussian, Inc., Pittsburgh PA, 1998.
- [23] W. J. Stevens, M. Krauss, H. Bosch and P. G. Jasien, *Can. J. Chem.* 70, 612, 1992.
- [24] W. Kohn, L. J. Sham, *Phys. Rev A* 140, 1133, 1965.
- [25] A. D. Becke, *Phys. Rev. A* 38, 3089, 1988.
- [26] C. Lee, W. Yang, R. G. Parr, *Phys. Rev B*, 37, 1988.
- [27] R. L. Flurry Jr., *Molecular Orbital Theory of Bonding in Organic Molecules*, Marcel Dekker, New York, 1968.
- [28] I. Turel, L. Golic, P. Bukovec and M. Gubina, *Journal of Inorganic Biochemistry* 71, 53, 1998.
- [29] I. Turel, P. Bukovec, M. Quiros, *Int. J. Pharm.* 152,59, 1997.
- [30] Yue Yang, Hongwei Gao, *Spectrochimica Acta part A* 85,303-309, 2012.
- [31] S.Sagdinc and S. Bayari, *Journal of Molecular Structure* 691, 107-113, 2004.
- [32] A. Yoshida, R. Moroi, *Anal. Sci.* 7, 351, 1991.
- [33] S.Sagdinc and S. Bayari, *Journal of Molecular Structure (THEOCHEM)* 668, 93-99, 2004.
- [34] I. Fleming *Frontier Orbitals and Organic Chemical Reactions*, Wiley, London, 1976.
- [35] A. Popova, E. Sokolova, S. Raicheva, M. Christov. *Corros. Sci.* 45, 33, 2003.
- [36] D. Zhang, L. Gao, G. Zhou, K.J. Lee. *J. Appl. Electrochem.* 38, 71, 2008.

- [37] G. Moretti, G. Quartarone, A. Tassan, A. Zingales. *Werkst. Korros.* 45, 641, 1994.
- [38] R.F. Villamil, P. Corio, J.C. Rubin, S.M. Agostinho. *J. Electroanal. Chem.* 472, 112, 1999.
- [39] R.F. Villamil, P. Corio, K. Lee. *J. Electroanal. Chem.* 535, 75, 2002.
- [40] E. Bayol, A.A. Gurten, M. Dursun, K. Kayakirilmaz. *Acta Phys. Chim. Sin.* 24, 2236, 2008.
- [41] O.K. Abiola, N.C. Oforka. part 1. *Mater. Chem. Phys.* 83, 315, 2004.
- [42] X. Li, S. Deng, H. Fu, T. Li. *Electrochim. Acta* 54, 4089, 2009.
- [43] P.C. Okafor, M.E. Ikpi, I.E. Uwah, E.E. Ebenso, U.J. Ekpe, S.A. Umoren. *Corros. Sci.* 50, 2310, 2008.
- [44] Y. Ren, Y. Luo, K. Zhang, G. Zhu, X. Tan. *Corros. Sci.* 50, 3147, 2008.
- [45] S.A. Umoren, I.B. Obot, E.E. Ebenso, P.C. Okafor, O. Ogbobe, E.E. Oguzie. *Anti-Corros. Methods Mater.* 53(5), 277, 2006.
- [46] L. Larabi, O. Benali, S.M. Mekelleche, Y. Harek. *J. Appl. Surf. Sci.* 253, 1371, 2006.
- [47] G. Gunasekaran, L.R. Chauhan. *Electrochim. Acta* 49, 4387, 2004.
- [48] S.S. Abdel-Rehim, O.A. Hazzazi, M.A. Amin, K.F. Khaled. *Corros. Sci.* 50, 2258, 2008.
- [49] S.S. Abdel-Rehim, K.F. Khaled, N.S. Abd-Elshafi. *Electrochim. Acta* 51, 3269, 2006.
- [50] A.S. Fouda, M.N. Moussa, F.I. Taha, A.I. Elneanaa. *Corros. Sci.* 26, 719, 1986
- [51] F. Bentiss, M. Traisnel, M. Lagrene. *Appl. Surf. Sci.* 161, 194, 2000.
- [52] N. Hackerman, E.S. Snively, J.S. Payne. *J. Electrochem. Soc.* 113, 677, 1967.
- [53] T. Murakawa, S. Nagaura, N. Hackerman. *Corros. Sci.* 7, 79, 1967.
- [54] D. Schweinsberg, G. George, A. Nanayakara, D. Steiner. *Corros. Sci.* 28, 33, 1988.
- [55] G.M. Mu, T.P. Zhao, M. Liu, T. Gu. *Corrosion* 52, 853, 1969.

IJSER